Environmental Science & Technology

pubs.acs.org/est

Article

Brownness of Organic Aerosol over the United States: Evidence for Seasonal Biomass Burning and Photobleaching Effects

Lung-Wen Antony Chen,* Judith C. Chow, Xiaoliang Wang, Junji Cao, Jingqiu Mao, and John G. Watson

Cite This: https://doi.org/10.1021/acs.est.0c08706

Read Online

ACCESS | Metrics & More | Article Recommendations | Supporting Information

ABSTRACT: Light-absorptivity of organic aerosol may play an important role in visibility and climate forcing, but it has not been assessed as extensively as black carbon (BC) aerosol. Based on multiwavelength thermal/optical analysis and spectral mass balance, this study quantifies BC for the U.S. Interagency Monitoring of Protected Visual Environments (IMPROVE) network while developing a brownness index (γ_{Br}) for non-BC organic carbon (OC*) to illustrate the spatiotemporal trends of light-absorbing brown carbon (BrC) content. OC* light absorption efficiencies range from 0 to 3.1 m^2 gC^{-1} at 405 nm, corresponding to the lowest and highest BrC content of 0 and 100%, respectively. BC, OC*, and γ_{Br} explain >97% of the variability of measured spectral light absorption (405−980 nm) across 158 IMPROVE sites. Network-average OC* light absorptions at 405 nm are 50 and 28% those for BC over rural and urban areas, respectively. Larger organic fractions of light absorption occur in winter, partially due to higher organic brownness. Winter γ_{Br} exhibits a dramatic regional/urban−rural contrast consistent with anthropogenic BrC emissions from residential wood combustion. The spatial differences diminish to uniformly low γ_{Br} in summer, suggesting effective BrC photobleaching over the midlatitudes. An empirical relationship between BC, ambient temperature, and γ_{Br} is established, which can facilitate the incorporation of organic aerosol absorptivity into climate and visibility models that currently assume either zero or static organic light absorption efficiencies.

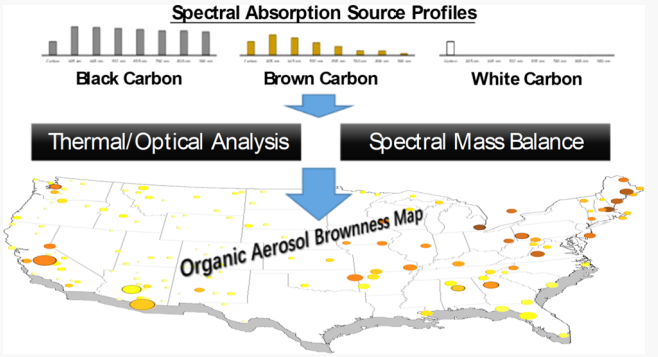

KEYWORDS: *brown carbon, black carbon, white carbon, aerosol aging, IMPROVE network, hybrid environmental receptor model*

Downloaded via UNIV OF ALASKA FAIRBANKS on June 24, 2021 at 21:53:35 (UTC).
See https://pubs.acs.org/sharingguidelines for options on how to legitimately share published articles.

INTRODUCTION

Carbonaceous aerosols affect the Earth's climate, tropospheric chemistry, and visibility.[1−3] Carbon accounts for 20−50% of fine aerosol mass on a global scale, but this fraction can be as much as 80% in urban environments due to energy-related fossil and biofuel combustion.[4,5] Smoke from wildland fires that consume millions of acres of vegetation each year consists mainly of carbonaceous material.[6−9] Complex photo-, gaseous-, and aqueous-phase chemistry occurring in the atmosphere continuously creates secondary organic aerosol (SOA) and transforms existing carbonaceous aerosol into more aged forms.[10] The wide range of chemical compounds in carbonaceous aerosol challenges chemical transport models (CTMs) to accurately predict their abundances, spatiotemporal variations, and effects.[11]

The direct radiative effects of carbonaceous aerosol are often assessed through its two main components, black carbon (BC) and organic carbon (OC), that have distinct optical properties. BC represents the thermally refractory and chemically inert fraction of carbonaceous aerosol resulting from high-temperature combustion and is commonly quantified through aerosol light absorption.[12] With a quasi-graphitic structure, BC absorbs sunlight with the mass absorption efficiency (MAE) following a power function of wavelength (λ)

$$MAE_{BC,\lambda} = C \times \lambda^{-AAE} \quad (1)$$

where C is a constant and AAE is the absorption Angström exponent often assumed to be ~1 for bulk BC.[13,14] OC is the counterpart of BC in the form of organic matter. Until recently, visibility and climate models have assumed OC to be purely light-scattering, much like secondary sulfate and nitrate aerosols.[1,15−17] Mounting evidence indicates the presence of light-absorbing organic compounds in OC. These compounds are often referred to as brown carbon (BrC) since their MAEs skew more toward shorter wavelengths than BC (i.e., AAEs > 1), and thus, they appear yellow/brown rather than black.[18]

Received: December 24, 2020
Revised: May 28, 2021
Accepted: June 1, 2021

ACS Publications © XXXX American Chemical Society

Biomass burning, particularly the smoldering phase with low combustion efficiency, is known to generate primary BrC and volatile precursors that form light-absorbing SOA as the smoke ages.[19−23] Biogenic SOA formed in the absence of nitrogen oxides and ammonia is not typically light-absorbing.[24,25] Past studies have not deemed fossil-fuel combustion to be an important source of BrC, although there is recent evidence of urban BrC associated with motor vehicle and/or coal combustion emissions.[26,27] The chemical nature of BrC is uncertain, but it likely consists of highly oxygenated and branched aromatic structures similar to humic-like substances.[24,28,29] Saleh[30] proposed four classes of BrC ranging from the very weakly absorptive to strongly absorptive according to their MAEs and AAEs. Each BrC class has an AAE greater than unity, although the spectral dependence of ambient BrC absorption across the visible region may not be explained by a single AAE.

Incorporating BrC in CTMs could alter the sign and magnitude of aerosol radiative forcing estimates.[31−33] While BC and OC are commonly quantified as part of ambient and source measurements, there has not been a well-accepted method for quantifying BrC along with its counterpart, the non-light-absorbing portion of OC also known as white carbon (WtC). Most often BrC abundances stemmed from measured spectral absorptivity of OC and presumed BrC light absorption efficiencies.[34] Instead of quantifying BrC, Saleh et al.[21] assessed brownness of organics in biomass burning smoke based on the imaginary part of the refractive index and its spectral dependence, but such an assessment has not been widely extended to other source emissions or ambient aerosols. Once in the atmosphere, "whitening" of OC occurs under sunlight-induced photobleaching that destroys specific chromophores.[35−37] Models must also address the dynamic change of organic aerosol brownness when predicting its climate effects.

For decades, several long-term aerosol speciation networks around the world have been reporting total carbon (TC) concentrations and the division of OC and elemental carbon (EC) within TC by thermal/optical analysis (TOA).[38−40] EC often serves as a surrogate for BC,[15,41] although it may deviate from BC quantified directly through light absorption measurements.[42,43] Measures for BC and organic brownness, when added to the networks, can generate useful data sets to further constrain CTMs for climate assessment. The Interagency Monitoring of Protected Visual Environments (IMPROVE) network collects $PM_{2.5}$ [particulate matter (PM) with aerodynamic diameter < 2.5 μm] on filters at ∼160 rural and urban sites across the United States (US), quantifying TC, OC, and EC by TOA with the IMPROVE_A protocol.[44,45] Since 2016, a multiwavelength TOA procedure has been applied to IMPROVE samples, which measures sample light absorption concurrently at seven wavelengths between 405 and 980 nm. This allows development of the first nationwide, continuous data set that registers BC and organic light absorption.

This paper uses the IMPROVE data set to demonstrate that light absorption by organic aerosols in US rural and urban areas can be modeled by a single brownness index indicative of the BrC proportion in OC. The spatiotemporal variations of this brownness index highlight the effects of season-dependent anthropogenic emissions and photobleaching on organic light absorption across the visible spectrum. An empirical relationship among the brownness index, BC levels, and ambient temperature is proposed for CTMs and climate models to constrain aerosol radiative forcing simulations.

MATERIALS AND METHODS

The multiwavelength TOA (DRI model 2015, Magee Scientific, Berkeley, CA, USA) heats $PM_{2.5}$ samples at predefined temperature stages following the IMPROVE_A protocol while monitoring filter reflectance and transmittance at seven wavelengths (405, 445, 532, 635, 780, 808, and 980 nm) throughout the analysis.[46−48] Both reflectance (R) and transmittance (T) decrease after the first four temperature steps (140, 280, 480, and 580 °C) in a pure helium atmosphere due to organic pyrolysis. R and T return to their initial values (i.e., the split point) during the last three temperature steps (580, 740, and 840 °C) in 98% helium−2% oxygen atmosphere as the pyrolyzed carbon and EC are gradually oxidized. OC and EC are defined as carbon evolved before and after the split point for the 635 nm reflectance, respectively, while TC is the sum of OC and EC. The TOA OC−EC split is based on three assumptions on OC: (1) OC absorptivity is negligible at ∼635 nm; (2) OC is either evolved or pyrolyzed (i.e., cannot remain intact) prior to the introduction of oxygen; and (3) pyrolyzed OC is equivalent to EC with respect to the reflectance or transmittance responses.[49,50] Deviations from these assumptions in some samples may result in EC overestimates or underestimates.[51−53]

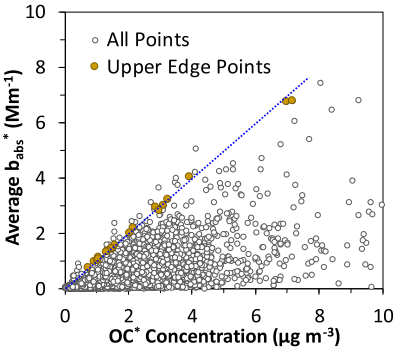

Figure 1. Scatter plot of non-BC light absorption (b_{abs}^{*}) vs organic carbon (OC*). Values were derived from multiwavelength carbon analysis of IMPROVE samples. b_{abs}^{*} are averages over seven wavelengths. The 20 samples highlighted in brown (with the top 0.3−0.5 percentile of b_{abs}^{*}/[OC*] ratios) were selected as BrC references to construct the BrC spectral absorption profile.

A total of 20,383 valid carbon analyses were conducted for the IMPROVE network in 2016. Around 11%, or 2339, of them were replicates for determining the carbon and optical measurement precisions.[54] Ten IMPROVE sites were outside the continental United States, with four in Alaska, two in Hawaii, two in Canada, one in the Virgin Islands, and one in South Korea. Virgin Islands and South Korean sites were excluded from this study. Site information is available on the IMPROVE website: http://vista.cira.colostate.edu/Improve/monitoring-site-browser/.

Loading Correction. Light attenuation (ATN) was first calculated from the filter transmittance prior to (T_i) and after (T_f) heating that removes carbon deposits from the filter, thus

$$\mathrm{ATN} = -\ln\left(\frac{T_i}{T_f}\right) \quad (2)$$

https://doi.org/10.1021/acs.est.0c08706
Environ. Sci. Technol. XXXX, XXX, XXX−XXX

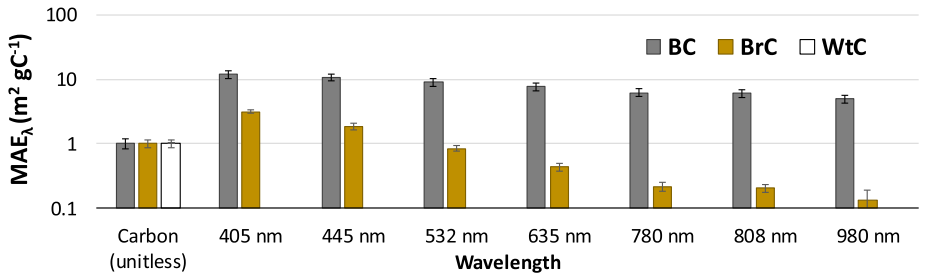

Figure 2. Spectral absorption profiles of black carbon (BC), brown carbon (BrC), and white carbon (WtC). The profiles were derived from IMPROVE samples in terms of carbon and wavelength-dependent light absorption coefficients normalized to the carbon mass (i.e., mass absorption efficiencies [MAE$_\lambda$]). Note MAE$_\lambda$ = 0 for WtC. Error bars indicate uncertainties in the profiles.

ATN is not linearly related to light absorption by the aerosol deposit due to multiple scattering and loading effects.[55,56] Chen et al.[46] outlined a spectral loading correction to convert ATN at each of the seven wavelengths to bulk aerosol absorption using diesel soot as a reference material. Diesel soot showed better correlations between EC quantified by TOA and light absorption quantified by a photoacoustic method than other source or ambient samples owing to less pyrolyzed carbon that influences the OC−EC split.[57] Different TOA protocols report consistent EC measurements from diesel soot.[52,58] In Chen et al.,[46] light absorption caused by diesel soot was estimated from EC, using a MAE$_{635nm}$ of 7.4 m^2 gC^{-1} and an AAE of 1. Relating the light absorption with measured ATN at the same wavelength established wavelength-specific conversion curves, which were then applied to all samples for the loading correction.

Since the correction likely depends on the sampling substrate, face velocity, and thus the particle penetration depth, alternative conversion curves for the IMPROVE network were established using 21 IMPROVE samples closely resembling diesel soot. These samples showed the highest EC/TC ratios of 0.52−0.84, with EC dominated by carbon evolving at high temperatures ≥ 740 °C (73 ± 25%). Analytical artifacts resulting from pyrolysis were minimal in these samples, as evidenced by a good agreement (within ±10%) between EC based on reflectance versus transmittance. The measured attenuations of these samples correlated well (r^2 > 0.9) with light absorptions ($b_{abs,\lambda}$) estimated from EC via second-order polynomial regressions (Figure S1), which defined the conversion curves. These curves were then applied to all IMPROVE samples to yield loading-corrected $b_{abs,\lambda}$ measurements (in Mm^{-1}). Standard errors of the regression coefficients were propagated into the uncertainties of $b_{abs,\lambda}$.

Spectral Absorption Profiles. A three-component model is applied to explain the variability in TC and $b_{abs,\lambda}$

$$[TC] = [BC] + [BrC] + [WtC] \quad (3)$$

$$b_{abs,\lambda} = MAE_{BC,\lambda} \times [BC] + MAE_{BrC,\lambda} \times [BrC] + MAE_{WtC,\lambda} \times [WtC] \quad (4)$$

where the brackets indicate concentrations in μg m^{-3}. Equations 3 and 4, referred to as "spectral mass balance", are analogous to the chemical mass balance (CMB) equation, which can be solved for [BC], [BrC], and [WtC] by an effective-variance (EV) least-squares minimization algorithm when all MAEs are known or less definitively by positive matrix factorization when MAEs are unknown.[59−61] In this case, the substance-specific MAE$_\lambda$ and associated uncertainties constitute a "spectral (source) profile" normalized to the carbon mass. Since BrC light absorption is minor in diesel soot, compositing MAE$_{BC,\lambda}$ for the 21 reference samples (i.e., from $b_{abs,\lambda}$/[EC]) produces an effective BC spectral profile with the mean MAE$_{BC,\lambda}$ as the profile values and standard deviations as the profile uncertainties. By definition, MAE$_{WtC,\lambda}$ is zero. The BrC spectral profile is then the only unknown profile in eq 4.

Ideally, a BrC spectral profile would be constructed from model BrC compounds or ambient samples containing exclusively BrC. The task is complicated by the wide range of BrC chemical structures and optical properties. Alternatively, CMB problems with a mix of known and unknown source profiles can be solved by the hybrid environmental receptor model (HERM) with a generalized EV algorithm[62,63] detailed in the Supporting Information. Herein, HERM utilizes the BC and WtC spectral profiles as constraints to calculate the BrC spectral profile along with BC, BrC, and WtC contributions. The model accounts for >97% of the TC and $b_{abs,\lambda}$ variability. It does not, however, provide a definite partition between BrC and WtC mass due to the lack of optical constraints on BrC. Figure 1 shows the scatter plot of average b^*_{abs} (i.e., $\overline{b^*_{abs,\lambda}}$) versus [OC*] where the asterisk indicates that BC contributions, as estimated by HERM, have been subtracted from $b_{abs,\lambda}$ and TC. OC* is TC minus BC, distinguished from OC quantified directly by TOA (i.e., OC = TC − EC). The difference between [OC] and [OC*] is the same as the difference between [EC] and [BC]. A clear upper boundary in Figure 1 corresponds to OC* that has the highest MAE and thus "brownness". For the three-component model (eqs 3 and 4), this would indicate OC* containing exclusively BrC. Other points below the boundary line suggest a mixture of BrC and WtC, leading to lower MAEs.

To exclude outliers, 20 samples in the top 0.3−0.5 percentile of $\overline{b^*_{abs,\lambda}}$/[OC*] ratio with [OC*] > 0.75 μg m^{-3} were identified to represent the upper boundary in Figure 1. From these samples, effective MAE$_{BrC,\lambda}$ were calculated to form a BrC spectral profile. Figure 2 compares the BC, BrC, and WtC spectral absorption profiles, where small uncertainties (5−15%, except for 43% at MAE$_{BrC,980nm}$ due to low signals) reflect consistency among samples forming the profiles. AAE for the BrC profile is 3.6 between 405 and 980 nm but 4.8 between 405 and 532 nm, which, combined with a MAE$_{BrC,532nm}$ of 0.84 m^2 gC^{-1}, is consistent with the optical properties of "moderately absorptive BrC".[30]

Carbon Mass Apportionment and Brownness Calculation. Applying the three spectral profiles to apportion TC and $b_{abs,\lambda}$ by HERM using the EV-CMB mode results in good fits to the data (i.e., r^2 > 0.97 for each wavelength of $b_{abs,\lambda}$; and

https://doi.org/10.1021/acs.est.0c08706
Environ. Sci. Technol. XXXX, XXX, XXX−XXX

Table 1. IMPROVE Carbon Fractions (TC, EC, BC, and OC* in μg m^{-3}), Organic Brownness Index (γ_{Br}), and Light Absorption (b_{abs} in Mm^{-1}) by Site Type and Season in 2016[a]

site type	season	TC	EC	BC	OC*	γ_{Br}	$b_{abs,BC(405nm)}$	$b_{abs,OC*(405nm)}$	$b_{abs,BC(532nm)}$	$b_{abs,OC*(532nm)}$
rural	annual	1.05	0.09	0.08	0.97	0.17	0.99	0.50	0.76	0.13
		(0.19−8.4)	(0−0.3)	(0.01−0.3)	(0.18−8.21)	(0.05−0.42)	(0.14−3.6)	(0.04−1.77)	(0.11−2.74)	(0.01−0.48)
	winter	0.65	0.09	0.08	0.57	0.27	0.96	0.61	0.73	0.16
		(0.14−3.15)	(0−0.57)	(0.01−0.55)	(0.11−2.6)	(0.06−0.76)	(0.11−6.59)	(0.03−3.75)	(0.08−5.02)	(0.01−1.01)
	spring	1.20	0.09	0.08	1.12	0.16	0.94	0.47	0.72	0.13
		(0.21−30.9)	(0.01−0.73)	(0.02−0.44)	(0.19−30.6)	(0.03−0.53)	(0.19−5.2)	(0.03−4.89)	(0.15−3.96)	(0.01−1.32)
	summer	1.32	0.09	0.09	1.23	0.08	1.02	0.32	0.78	0.09
		(0.19−7.49)	(0−0.7)	(0.01−0.3)	(0.18−7.2)	(0.02−0.21)	(0.1−3.64)	(0.02−2.9)	(0.08−2.77)	(0.01−0.78)
	fall	1.04	0.10	0.09	0.95	0.17	1.03	0.57	0.79	0.15
		(0.19−3.83)	(0.01−0.35)	(0.01−0.3)	(0.18−3.66)	(0.03−0.41)	(0.1−3.56)	(0.04−2.62)	(0.08−2.71)	(0.01−0.71)
urban	annual	2.69	0.57	0.62	2.08	0.30	7.35	2.03	5.59	0.55
		(1.8−3.49)	(0.38−0.74)	(0.47−0.8)	(1.33−2.93)	(0.2−0.42)	(5.6−9.54)	(1.52−3.28)	(4.26−7.26)	(0.41−0.88)
	winter	3.64	0.81	0.87	2.78	0.48	10.37	3.87	7.89	1.04
		(1.57−6.67)	(0.36−1.51)	(0.37−1.46)	(1.2−5.25)	(0.30−0.74)	(4.42−17.4)	(2.2−7.88)	(3.37−13.2)	(0.59−2.12)
	spring	2.09	0.43	0.46	1.63	0.24	5.45	1.21	4.15	0.33
		(1.66−3.02)	(0.24−0.67)	(0.23−0.72)	(1.22−2.49)	(0.12−0.33)	(2.79−8.55)	(0.54−1.63)	(2.12−6.51)	(0.15−0.44)
	summer	2.06	0.38	0.41	1.65	0.12	4.95	0.65	3.77	0.17
		(1.26−2.93)	(0.19−0.63)	(0.24−0.71)	(1.02−2.37)	(0.05−0.21)	(2.9−8.44)	(0.18−1.23)	(2.21−6.43)	(0.05−0.33)
	fall	2.97	0.66	0.72	2.25	0.35	8.63	2.39	6.57	0.65
		(2.02−4.05)	(0.42−1.02)	(0.58−1.13)	(1.44−3.33)	(0.22−0.49)	(6.91−13.5)	(1.89−3.6)	(5.26−10.2)	(0.51−0.97)
all sites	annual	1.14	0.12	0.11	1.03	0.18	1.36	0.58	1.03	0.16
		(0.19−8.4)	(0−0.74)	(0.01−0.8)	(0.18−8.21)	(0.05−0.42)	(0.14−9.54)	(0.04−3.28)	(0.11−7.26)	(0.01−0.88)

[a]Average values and ranges (in bracket) are based on site-specific means (annual or seasonal) across 158 sites, excluding two IMPROVE sites in Virgin Islands and South Korea. Refer to Table S2 for standard deviations and standard errors. TC: total carbon. EC: elemental carbon. BC: black carbon. OC*: non-BC organic carbon, derived from TC minus BC. Winter: December-February. Spring: March-May. Summer: June-August. Fall: September-November.

https://doi.org/10.1021/acs.est.0c08706
Environ. Sci. Technol. XXXX, XXX, XXX−XXX

an overall Chi-square, a measure of fitting residuals = 0.12). HERM also calculates wavelength- and sample-specific Chi-squares, denoted by χ_i^2 and χ_k^2, respectively, as well as uncertainties of the carbon apportionment for each sample[62] (see the Supporting Information). All χ_i^2 are less than 0.5, and only 1.5% of χ_k^2 exceed 0.5 (Table S1), indicating poor fits and large uncertainties in the calculated [BC] and [BrC] for these samples. Uncertainties may result from both measurement errors and deviations from the model assumptions for specific samples. Although several studies report varying BrC spectral dependence,[64,65] including more than one class of BrC in this study does not improve the model performance.

It is meaningful to define the brownness index (γ_{Br}) based on the [BrC]/[OC*] ratio. γ_{Br} ranks OC* by its effective BrC fraction, with γ_{Br} of 0 and 1 corresponding to exclusively WtC and BrC, respectively. Since the OC* MAE is also proportional to γ_{Br} (i.e., $MAE_{OC^*,\lambda} = \gamma_{Br} \times MAE_{BrC,\lambda}$), this index allows intra-/intersite comparisons to investigate how organic aerosol absorptivity varies in time and space. In scenarios where multiple classes of BrC are required to explain the OC* spectral absorption, each BrC class may be assigned a γ_{Br} (i.e., $\gamma_{Br,j}$ with j = 1, 2, ... for the mass fraction of class j in OC*) in order to construct the OC* MAE, thus $MAE_{OC^*,\lambda} = \sum_j \gamma_{Br,j} \times MAE_{BrC_j,\lambda}$.

All derivations here, including γ_B, are bulk properties measured on a filter deposit. Absorptions by different components are assumed to be additive, and deviations from this assumption, such as effects of particle size and internal mixing, have been addressed by the loading correction for a highly diffusive filter material.[46,66,67] Constructing the actual organic aerosol b_{abs} in the atmosphere would require more complex optical models taking into account the refractive index, particle size, and mixing of various aerosol components.[68,69]

RESULTS AND DISCUSSION

The results reported here are based on 18,044 filter samples acquired from 158 IMPROVE sites in the United States and Canada every third day between January 1 and December 29, 2016. Although the IMPROVE network mainly represents a regional background, it contains urban sites in eight cities including Atlanta, Birmingham, Detroit, Fresno, Nogales, Phoenix, Pittsburg, and Seattle. Over the network, [BC] averaged 0.11 ± 0.14 $\mu g\ m^{-3}$, similar to the average [EC] of 0.12 ± 0.13 $\mu g\ m^{-3}$ from TOA (Table 1, with standard deviations and standard errors shown in Table S2). Within individual sites, [BC] correlates with [EC], with r^2 ranging from 0.31 to 0.99 and >0.80 for half of the sites. Site-average [BC] and [EC] agree within a factor of 2 (Figure 3). Larger deviations are found when EC concentrations are often below the lower quantifiable limit (0.1 $\mu g\ m^{-3}$). The non-BC fraction of TC (i.e., OC*) averages 1.03 ± 0.95 $\mu g\ m^{-3}$. Site-average γ_{Br} ranges from 0.02 to 0.76 (Table 1) inferring MAE_{OC^*} of 0.1−2.4 $m^2\ gC^{-1}$ at 405 nm and 0.02−0.64 $m^2\ gC^{-1}$ at 532 nm.

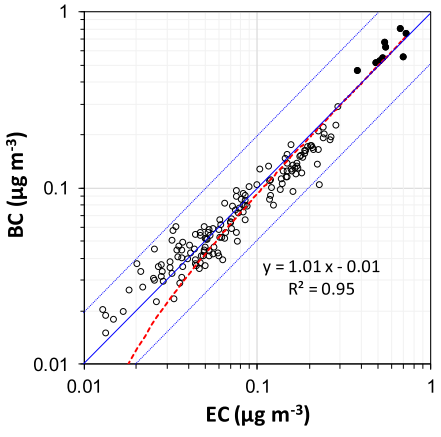

Figure 3. Comparison of BC and EC derived from multiwavelength carbon analysis. Each point represents the annual mean values for an IMPROVE site, with urban/rural sites marked by solid/open circles. The blue lines indicate 1:1, 1:2, and 2:1 ratios, and the red line is the linear regression.

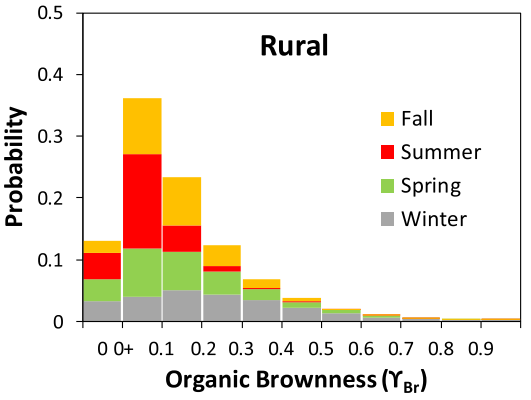

(a)

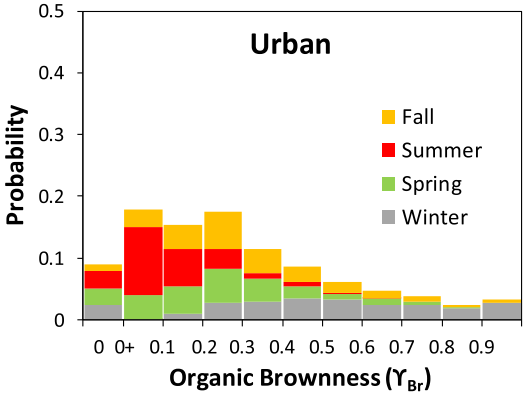

(b)

Figure 4. Season-dependent probability distribution of organic aerosol brownness across the IMPROVE network for (a) 150 rural and (b) 8 urban sites. Histograms are based on all samples in 2016, excluding those from Virgin Islands and South Korea. All the probabilities add up to 1, while the seasonal probabilities add up to 0.25. Winter: December-February. Spring: March-May. Summer: June-August. Fall: September-November.

Range and Variability of Organic Aerosol Brownness. A wide range of brownness is found in rural organic aerosols (Figure 4a). Overall, γ_{Br} < 0.2 for about three-fourths of the IMPROVE rural samples in 2016 with 13.1% containing only WtC (γ_{Br} = 0). The summer histogram is skewed toward lower γ_{Br} than those for other seasons. Browner OC* (e.g., γ_{Br} > 0.3) mostly occurred during winter months. Urban samples show a similar seasonal trend, although γ_{Br} further shifts to higher values, regardless of the season (Figure 4b). Around 10% of

https://doi.org/10.1021/acs.est.0c08706
Environ. Sci. Technol. XXXX, XXX, XXX−XXX

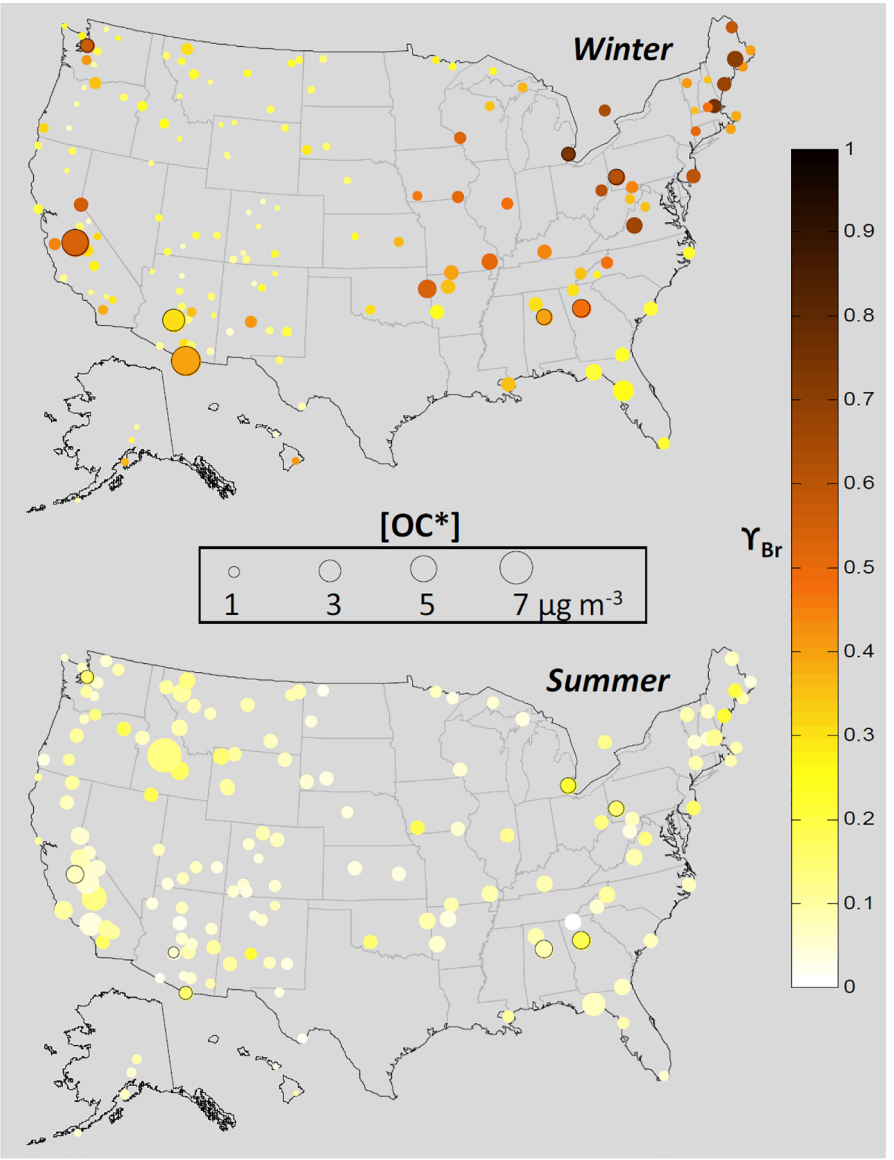

Figure 5. Spatial trends of non-BC organic carbon concentration, [OC*], and brownness (γ_{Br}). Data are from the IMPROVE network for winter (January, February, and December) and summer (June, July, and August) 2016. Circle size and color indicate season-average [OC*] and γ_{Br}, respectively. Bordered circles mark the urban sites.

the urban OC* have γ_{Br} greater than 0.7, indicating the dominance of BrC, in comparison with only 1% among the rural samples. Three-fourths of these urban samples ($\gamma_{Br} > 0.7$) were acquired in winter. The network-average γ_{Br} was 0.08 and 0.27 over summer and winter, respectively, for the rural sites but 0.12 (summer) and 0.48 (winter) for the urban sites (Table 1). Non-light-absorbing WtC appears to dominate the OC* mass most of the time.

Despite being browner in winter, [OC*] at the rural sites averaged lower in winter (0.57 $\mu g\ m^{-3}$) than in summer (1.23 $\mu g\ m^{-3}$) and other seasons (0.95−1.12 $\mu g\ m^{-3}$). This contrasts with BC or EC as their averages varied within ±10% among the seasons, being only slightly higher in fall (Table 1). BC has been widely used as a marker for bio- and/or fossil fuel combustion emissions[70,71] that also contain organic aerosols of various brownness. Major combustion sources that affect the rural IMPROVE sites are likely to be seasonally dependent, such as residential wood combustion (RWC) in winter versus wildfires in summer,[72] although no evidence suggests browner organic aerosol from the former than the latter. The seasonal variation of γ_{Br} may result from SOA formation and/or photobleaching, both of which promote WtC particularly in summer. In contrast, anthropogenic emissions in urban areas, such as engine exhaust and RWC, often cause higher pollution levels in winter due to a shallower surface mixing layer and increased heating demand.[73−75] For the urban IMPROVE sites, average [BC], [OC*], and γ_{Br} in winter were 2.1, 1.7, and 4.0 times, respectively, those measured in summer.

The spatial distributions of OC* concentration and brownness are further illustrated in Figure 5. During winter, rural sites in the eastern United States observed higher [OC*] than those in the western United States, while higher γ_{Br} (up to 0.76 on seasonal average) occurred primarily in the Northeast and Midwest regions. The brownness appears to reflect BrC from RWC as they share a similar spatial pattern.[76] Urban areas at lower latitudes (i.e., Atlanta, Birmingham, Nogales, and Phoenix) with minor RWC emissions also observed lower γ_{Br} (0.30−0.48) than those at higher/colder latitudes (Detroit,

https://doi.org/10.1021/acs.est.0c08706
Environ. Sci. Technol. XXXX, XXX, XXX−XXX

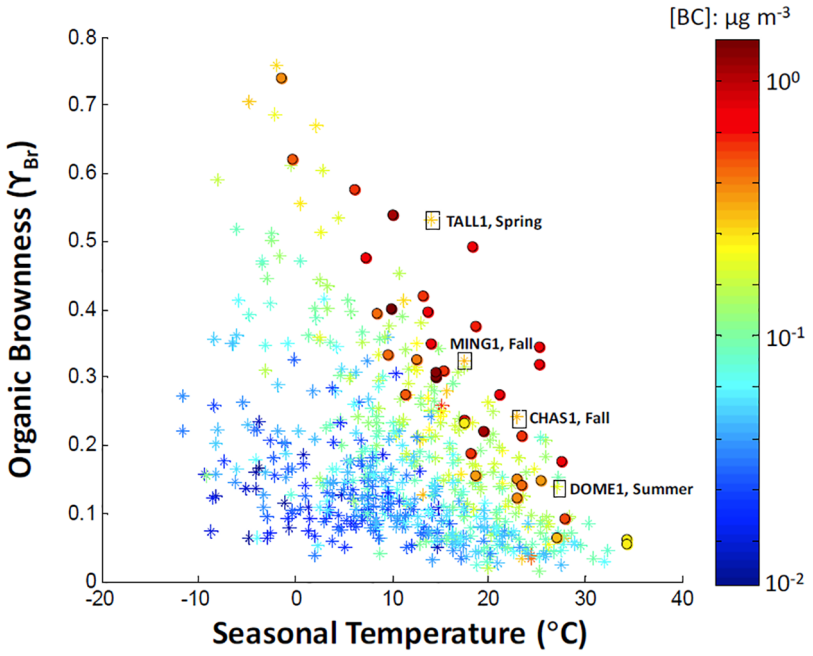

Figure 6. Seasonal average organic aerosol brownness (γ_{Br}) vs ambient temperature. Data represent the IMPROVE network in 2016. Color codes indicate concurrent BC concentrations. Stars and circles mark the rural and urban measurements, respectively, while squares denote rural high-[BC] events due to prescribed brush and forest fires. Temperature data were acquired from the PRISM Climate Group at Oregon State University (https://prism.oregonstate.edu/).

Fresno, Pittsburg, and Seattle; γ_{Br} = 0.54−0.74). However, γ_{Br} was higher at each urban site than at neighboring rural sites, even though RWC might account for a smaller fraction of organic aerosol within urban areas due to larger contributions from mobile sources.[77,78] Gasoline engines have been shown to be a potential source of BrC, with BrC emissions enhanced under low ambient temperatures.[79] Aerosol aging offers another explanation for the urban−rural contrast. As the rural sites are farther from sources, additional aging during transport could lower aerosol brownness even in winter.

Seasonal average γ_{Br} declined to 0.2 or less throughout the United States in summer, whereas the regional and urban−rural contrast mostly diminished (Figure 5). This is consistent with the absence of RWC contributions and more thorough atmospheric mixing. Elevated summertime SOA did not drive aerosol brownness. Furthermore, two sites impacted by intense wildfires, that is, Sawtooth National Forest (SAWT1) in Idaho and Domeland Wilderness (DOME1) in California, measured the highest OC* levels but only moderate γ_{Br} of 0.13−0.14. The relatively low brownness of summer biomass burning aerosol points to the possibility of rapid photobleaching that converts BrC into WtC within a short period of time as plumes travel from the source to receptor. Photobleaching may whiten urban BrC as efficiently, considering the much suppressed γ_{Br} (0.06−0.18) for the organic aerosols at Atlanta, Birmingham, Nogales, and Phoenix in summer compared with those in winter.

Predictive Factors for γ_{Br}. Taking ambient temperature as a surrogate of seasonal variations in atmospheric processes, such as solar radiation, photochemistry, and photobleaching intensity, it is plotted against γ_{Br} across all the IMPROVE sites and seasons in Figure 6. Each data point is also color-coded according to the average [BC] that marks the direct influence of combustion sources including RWC, wildfires, and urban anthropogenic emissions. Higher [BC] generally correspond to higher brownness in OC*, with the urban sites observing top seasonal BC and γ_{Br} levels for any temperature range. The upper edge of scatter in Figure 6 also contains a few rural high-[BC] events attributable to wildland fires, such as prescribed burning at Tallgrass Prairie National Preserve (TALL1, Kansas) in spring (γ_{Br} = 0.53), brush fires at Mingo (MING1, Missouri) and Chassahowitzka (CHAS1, Florida) National Wildlife Refuges in fall (γ_{Br} = 0.32 and 0.24, respectively), and a forest fire close to Domeland Wilderness (DOME1), California, in summer (γ_{Br} = 0.14). [BC] ranges between 0.2 and 0.3 μg m^{-3} among the four events. These findings corroborate that BrC mainly results from combustion emissions along with BC.

Regardless of the BC level, γ_{Br} decreases with the increase of ambient temperature and converges to a small range of 0.03−0.1 when the temperature exceeds 28 °C on a seasonal average. This includes sites heavily impacted by wildfires or traffic emissions and is consistent with photobleaching intensity increasing with temperature in both rural and urban environments. For instance, γ_{Br} for the TALL1, MING1, CHAS1, and DOME1 fire events varied in the reverse order of the corresponding seasonal temperature (14.0, 17.4, 22.9, and 27.1 °C, respectively) provided that their BC levels were similar (Figure 6). Higher temperatures can also cause larger biogenic emissions and thus SOA fractions in summer than winter,[80,81] further lowering the OA brownness. An empirical function of [BC] and temperature (T) is formulated, which explains ~60% of variability in seasonal γ_{Br} (r^2 = 0.61, see Figure S2) across the continental United States.

$$\gamma_{Br} = -a \times \log_{10}\left(\frac{[BC]}{[BC]_0}\right) \times (T - T_0) \quad (5)$$

The fitting coefficients with 95% confidence bounds: a = 0.010 (0.009, 0.011), $[BC]_0$ = 0.010 (0.008, 0.011) μg m^{-3},

https://doi.org/10.1021/acs.est.0c08706
Environ. Sci. Technol. XXXX, XXX, XXX−XXX

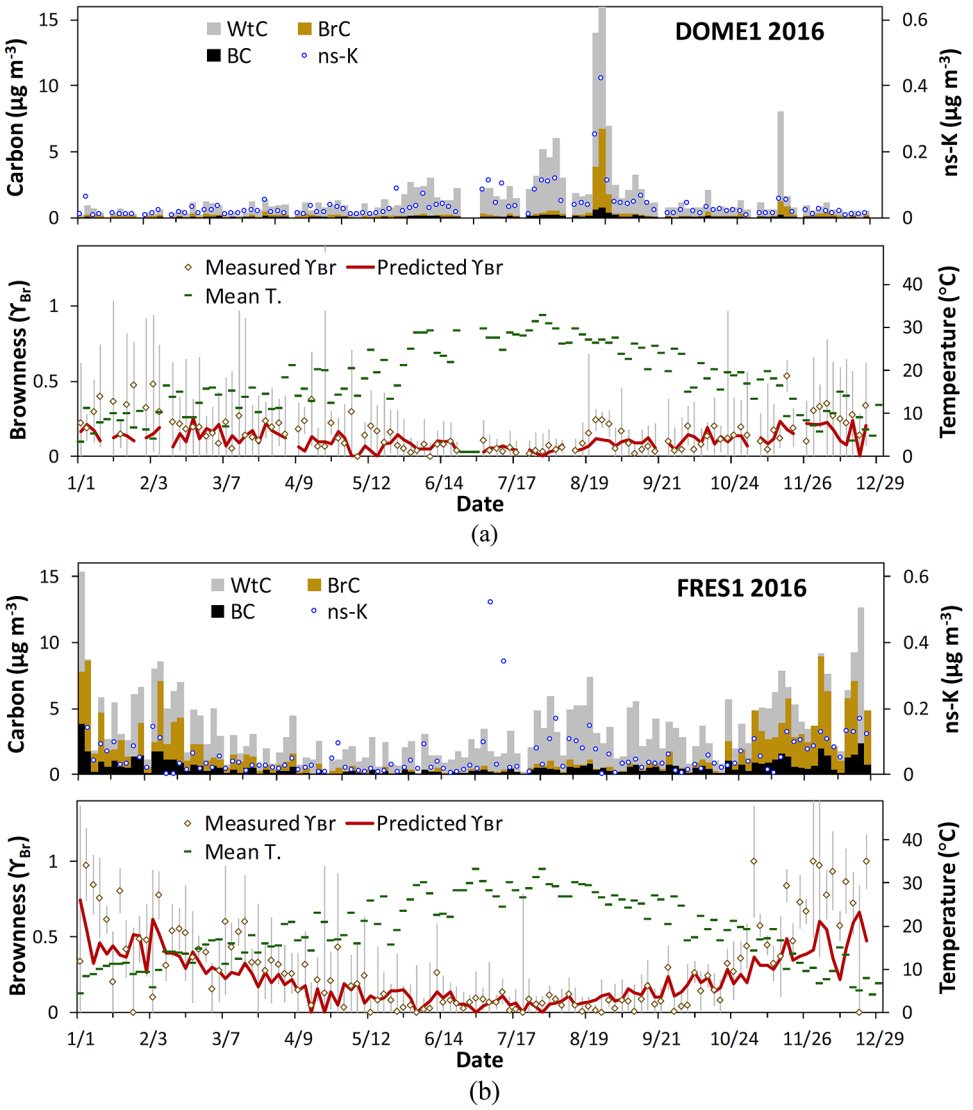

Figure 7. Time series of aerosol properties every third day in 2016. Data include carbon fractions (BC, BrC, and WtC), nonsoil potassium (ns-K), measured/predicted organic aerosol brownness (γ_{Br}), and daily mean temperature (T) at (a) Domeland Wilderness (DOME1), ~160 km southeast of Fresno, and (b) City of Fresno (FRES1) in central California.

and T_0 = 33 (31, 35) °C were calculated by the Matlab Curve Fitting Toolbox. A cross validation test using 30% of data selected randomly for model fitting yielded a predictivity of 61 (56, 65)% for the remaining 70% of the data (based on r^2 from 1,000 independent runs). Using a bisquare robust fitting[82] that down-weights points farther from the fitted line did not change the results significantly. If only temperature dependence is of concern (i.e., for constant [BC]), eq 5 can be simplified to

$$\gamma_{Br}(T) = \gamma_{Br}(0\ ^\circ\mathrm{C}) \times \left(1 - \frac{T}{33^\circ\mathrm{C}}\right) \quad (6)$$

The working range for eqs 5 and 6 is [BC]: 0.01−1 μg m^{-3} and T: −12−33 °C, where γ_{Br} doubles for every 10-fold increase of [BC] and decreases by ~3% of its value at 0 °C for every degree increase in temperature.

Rural and Urban Case Studies. Figure 7 shows time series of BC, OC*, and γ_{Br} at DOME1 and the most proximate urban site, FRES1 (Fresno, CA). Seasonal variations at the two sites are typical of those for rural and urban areas in the western United States. Moreover, both sites were impacted by several wildfires, particularly the Cedar Fire in Kern County starting mid-August.[83] Nonsoil potassium (ns-K) derived from potassium (K) and iron (Fe) concentrations, that is, [ns-K] = [K] − 0.37 × [Fe],[84] serves as a marker for biomass burning aerosol. Elevated [ns-K], [BC], and [OC*] over DOME1 and FRES1 in late July through mid-September corresponded to the wildfire impact. Similarly high ns-K levels showed up in winter only for FRES1, consistent with substantial RWC emissions.[73] BC correlated with ns-K strongly at DOME1 (r^2 = 0.81) but not as much at FRES1, even excluding two samples possibly influenced by fireworks in July (r^2 = 0.36) as fossil fuel combustion also contributes to BC at Fresno.

At the peak of Cedar Fire smoke impact, γ_{Br} ranged 0.02−0.04 at FRES1 (August 19−22) in comparison with 0.22−0.24 at DOME1 (August 22−28). Ambient temperatures were rather uniform during the period (daily mean: 26−30 °C; see Figure 7), but more aged smoke arrived at FRES1 than at DOME1 as a result of 4 times the transport distance (100 km vs 25 km). Aging promotes BrC photobleaching and mixing with weakly absorbing organic aerosols, thus lowering γ_{Br}. The

https://doi.org/10.1021/acs.est.0c08706
Environ. Sci. Technol. XXXX, XXX, XXX−XXX

dramatic difference between FRES1 aerosol brownness in August and December, despite similar ns-K levels, again corroborates the seasonal photobleaching intensity. Although eqs 5 and 6 were developed from seasonal average data, they appear to predict daily γ_{Br} within the estimated γ_{Br} uncertainty most of the time (Figure 7), when provided with daily [BC] and temperature as inputs. Larger biases between measured and predicted γ_{Br} can occur when a site experiences "fresh" biomass burning smoke such as DOME1 during the Cedar Fire and FRES1 during winter, where the nondynamic model tends to overestimate the photobleaching effect on γ_{Br}.

Light Absorption by OC* Versus BC. Light absorptions apportioned to organic aerosol ($b_{abs,OC*}$) are shown in Table 1. At 405 nm, rural $b_{abs,OC*}$ ranged from 0.04 to 1.8 Mm^{-1} annually with a network average of 0.50 ± 0.42 Mm^{-1}, which is ~50% of the BC absorption (average $b_{abs,BC}$ = 0.99 ± 0.65 Mm^{-1}). Seasonal $b_{abs,OC*}$ reached ~two-thirds of $b_{abs,BC}$ in winter and ~one-third in summer. The relative contribution of organic absorption was still significant at the urban sites (>25% of BC absorption on average), despite elevated BC levels. This was partially due to higher organic brownness over urban areas, especially in winter. As OC* absorptivity decreases sharply toward longer wavelengths, seasonal OC* absorptions at 532 nm were only 11−22 and 5−13% those of BC for the rural and urban IMPROVE sites, respectively.

Perspectives. This paper presents the first regional brownness map that will allow for ground-truthing model simulations or satellite retrievals of spectral aerosol light absorption (e.g., June et al.[85]). BC along with two classes of organic aerosol (i.e., BrC and WtC) with specific optical properties appear to explain the aerosol light absorption across the United States, while summertime atmospheric aging effectively converts BrC to WtC, thus reducing the brownness. Owing to a combination of extensive RWC and low temperatures, urban organic aerosols of the northeastern United States in winter exhibit the highest brownness. The organic light absorptions are generally lower than those of BC, but on network average can be up to two-thirds of BC absorption at 405 nm in winter. Whether additional BrC classes are required to account for organic absorptivity in other situations warrants further investigations and so does the empirical relationship between organic brownness, BC concentration, and ambient temperature found within the IMPROVE network. This can be accomplished by continuing the multiwavelength carbon analysis in the United States and expanding such measurements to other regional aerosol monitoring networks.

■ ASSOCIATED CONTENT

Supporting Information

The Supporting Information is available free of charge at https://pubs.acs.org/doi/10.1021/acs.est.0c08706.

Spectral conversion curves for filter loading correction; measured versus empirically predicted organic brownness indices; spectral mass balance model fitting performance measures; standard deviations and standard errors of annual and seasonal carbon concentrations, brownness indices, and light absorptions at 405 and 532 nm; and HERM formulations for the spectral mass balance (PDF)

HERM input/output data sets (XLSX)

■ AUTHOR INFORMATION

Corresponding Author

Lung-Wen Antony Chen − *Department of Environmental and Occupational Health, School of Public Health, University of Nevada, Las Vegas, Las Vegas, Nevada 89154, United States; Division of Atmospheric Sciences, Desert Research Institute, Reno, Nevada 89512, United States;* orcid.org/0000-0002-2311-7506; Email: antony.chen@unlv.edu

Authors

Judith C. Chow − *Division of Atmospheric Sciences, Desert Research Institute, Reno, Nevada 89512, United States; Institute of Earth Environment, Chinese Academy of Sciences, Xi'an 710061, China*

Xiaoliang Wang − *Division of Atmospheric Sciences, Desert Research Institute, Reno, Nevada 89512, United States*

Junji Cao − *Institute of Earth Environment, Chinese Academy of Sciences, Xi'an 710061, China;* Present Address: Institute of Atmospheric Physics, Chinese Academy of Sciences, Beijing, 100029, China.

Jingqiu Mao − *Department of Chemistry and Biochemistry, University of Alaska, Fairbanks, Alaska 99775, United States;* orcid.org/0000-0002-4774-9751

John G. Watson − *Division of Atmospheric Sciences, Desert Research Institute, Reno, Nevada 89512, United States; Institute of Earth Environment, Chinese Academy of Sciences, Xi'an 710061, China;* orcid.org/0000-0002-1752-6899

Complete contact information is available at: https://pubs.acs.org/10.1021/acs.est.0c08706

Notes

The authors declare no competing financial interest.

■ ACKNOWLEDGMENTS

This project was supported in part by the U.S. National Park Service IMPROVE Carbon Analysis Contract (P16PC0022) and National Science Foundation grants (AGS 2026821/2026824). The continuing development of HERM is supported by a joint venture between the University of Nevada, Las Vegas, and the Institute of Earth Environment, Chinese Academy of Sciences (Project ID: 2018001P). The authors appreciate valuable comments from three anonymous reviewers.

■ REFERENCES

(1) Intergovernmental Panel on Climate Change. *Climate Change 2013: The Physical Science Basis: Working Group I Contribution to the Fifth Assessment Report of the Intergovernmental Panel on Climate Change*; Cambridge University Press, 2014.

(2) Tie, X.; Madronich, S.; Walters, S.; Edwards, D. P.; Ginoux, P.; Mahowald, N.; Zhang, R.; Lou, C.; Brasseur, G. Assessment of the global impact of aerosols on tropospheric oxidants. *J. Geophys. Res.* **2005**, *110*, D03204.

(3) Watson, J. G. Visibility: Science and regulation. *J. Air Waste Manage. Assoc.* **2002**, *52*, 628−713.

(4) Jacobson, M. C.; Hansson, H.-C.; Noone, K. J.; Charlson, R. J. Organic atmospheric aerosols: Review and state of the science. *Rev. Geophys.* **2000**, *38*, 267−294.

(5) Kanakidou, M.; Seinfeld, J. H.; Pandis, S. N.; Barnes, I.; Dentener, F. J.; Facchini, M. C.; Van Dingenen, R.; Ervens, B.; Nenes, A.; Nielsen, C. J.; Swietlicki, E.; Putaud, J. P.; Balkanski, Y.; Fuzzi, S.; Horth, J.; Moortgat, G. K.; Winterhalter, R.; Myhre, C. E. L.; Tsigaridis, K.; Vignati, E.; Stephanou, E. G.; Wilson, J. Organic

aerosol and global climate modelling: a review. *Atmos. Chem. Phys.* **2005**, *5*, 1053−1123.
(6) Chen, L.-W. A.; Moosmüller, H.; Arnott, W. P.; Chow, J. C.; Watson, J. G.; Susott, R. A.; Babbitt, R. E.; Wold, C. E.; Lincoln, E. N.; Hao, W. M. Emissions from laboratory combustion of wildland fuels: Emission factors and source profiles. *Environ. Sci. Technol.* **2007**, *41*, 4317−4325.
(7) McMeeking, G. R.; Kreidenweis, S. M.; Baker, S.; Carrico, C. M.; Chow, J. C.; Collett, J. L.; Hao, W. M.; Holden, A. S.; Kirchstetter, T. W.; Malm, W. C.; Moosmüller, H.; Sullivan, A. P.; Wold, C. E. Emissions of trace gases and aerosols during the open combustion of biomass in the laboratory. *J. Geophys. Res.* **2009**, *114*, D19210.
(8) Jaffe, D. A.; O'Neill, S. M.; Larkin, N. K.; Holder, A. L.; Peterson, D. L.; Halofsky, J. E.; Rappold, A. G. Wildfire and prescribed burning impacts on air quality in the United States. *J. Air Waste Manage. Assoc.* **2020**, *70*, 583−615.
(9) Altshuler, S. L.; Zhang, Q.; Kleinman, M. T.; Garcia-Menendez, F.; Moore, C. T.; Hough, M. L.; Stevenson, E. D.; Chow, J. C.; Jaffe, D. A.; Watson, J. G. Critical Review Discussion: Wildfire and prescribed burning impacts on air quality in the United States. *J. Air Waste Manage. Assoc.* **2020**, *70*, 961.
(10) Jimenez, J. L.; Canagaratna, M. R.; Donahue, N. M.; Prevot, A. S.; Zhang, Q.; Kroll, J. H.; DeCarlo, P. F.; Allan, J. D.; Coe, H.; Ng, N. L.; Aiken, A. C. Evolution of organic aerosols in the atmosphere. *Science* **2009**, *326*, 1525−1529.
(11) Simpson, D.; Yttri, K. E.; Klimont, Z.; Kupiainen, K.; Caseiro, A.; Gelencsér, A.; Pio, C. A.; Puxbaum, H.; Legrand, M. Modeling carbonaceous aerosol over Europe: Analysis of the CARBOSOL and EMEP EC/OC campaigns. *J. Geophys. Res.: Space Phys.* **2007**, *112*, D23S14.
(12) Watson, J. G.; Chow, J. C.; Chen, L.-W. A. Summary of organic and elemental carbon/black carbon analysis methods and intercomparisons. *Aerosol Air Qual. Res.* **2005**, *5*, 65−102.
(13) Virkkula, A.; Ahlquist, N. C.; Covert, D. S.; Arnott, W. P.; Sheridan, P. J.; Quinn, P. K.; Coffman, D. J. Modification, calibration and a field test of an instrument for measuring light absorption by particles. *Aerosol Sci. Technol.* **2005**, *39*, 68−83.
(14) Moosmüller, H.; Chakrabarty, R. K.; Ehlers, K. M.; Arnott, W. P. Absorption Ångström coefficient, brown carbon, and aerosols: basic concepts, bulk matter, and spherical particles. *Atmos. Chem. Phys.* **2011**, *11*, 1217−1225.
(15) Pitchford, M.; Malm, W.; Schichtel, B.; Kumar, N.; Lowenthal, D.; Hand, J. Revised algorithm for estimating light extinction from IMPROVE particle speciation data. *J. Air Waste Manage. Assoc.* **2007**, *57*, 1326−1336.
(16) Leibensperger, E. M.; Mickley, L. J.; Jacob, D. J.; Chen, W.-T.; Seinfeld, J. H.; Nenes, A.; Adams, P. J.; Streets, D. G.; Kumar, N.; Rind, D. Climatic effects of 1950−2050 changes in US anthropogenic aerosols−Part 1: Aerosol trends and radiative forcing. *Atmos. Chem. Phys.* **2012**, *12*, 3333−3348.
(17) Fiore, A. M.; Naik, V.; Spracklen, D. V.; Steiner, A.; Unger, N.; Prather, M.; Bergmann, D.; Cameron-Smith, P. J.; Cionni, I.; Collins, W. J.; Dalsøren, S.; Eyring, V.; Folberth, G. A.; Ginoux, P.; Horowitz, L. W.; Josse, B.; Lamarque, J.-F.; MacKenzie, I. A.; Nagashima, T.; O'Connor, F. M.; Righi, M.; Rumbold, S. T.; Shindell, D. T.; Skeie, R. B.; Sudo, K.; Szopa, S.; Takemura, T.; Zeng, G. Global air quality and climate. *Chem. Soc. Rev.* **2012**, *41*, 6663−6683.
(18) Andreae, M. O.; Gelencsér, A. Black carbon or brown carbon? The nature of light-absorbing carbonaceous aerosols. *Atmos. Chem. Phys.* **2006**, *6*, 3131−3148.
(19) Chakrabarty, R. K.; Moosmüller, H.; Chen, L.-W. A.; Lewis, K.; Arnott, W. P.; Mazzoleni, C.; Dubey, M. K.; Wold, C. E.; Hao, W. M.; Kreidenweis, S. M. Brown carbon in tar balls from smoldering biomass combustion. *Atmos. Chem. Phys.* **2010**, *10*, 6363−6370.
(20) Saleh, R.; Hennigan, C. J.; McMeeking, G. R.; Chuang, W. K.; Robinson, E. S.; Coe, H.; Donahue, N. M.; Robinson, A. L. Absorptivity of brown carbon in fresh and photo-chemically aged biomass-burning emissions. *Atmos. Chem. Phys.* **2013**, *13*, 7683−7693.
(21) Saleh, R.; Robinson, E. S.; Tkacik, D. S.; Ahern, A. T.; Liu, S.; Aiken, A. C.; Sullivan, R. C.; Presto, A. A.; Dubey, M. K.; Yokelson, R. J.; Donahue, N. M.; Robinson, A. L. Brownness of organics in aerosols from biomass burning linked to their black carbon content. *Nat. Geosci.* **2014**, *7*, 647−650.
(22) Gilardoni, S.; Massoli, P.; Paglione, M.; Giulianelli, L.; Carbone, C.; Rinaldi, M.; Decesari, S.; Sandrini, S.; Costabile, F.; Gobbi, G. P.; Pietrogrande, M. C.; Visentin, M.; Scotto, F.; Fuzzi, S.; Facchini, M. C. Direct observation of aqueous secondary organic aerosol from biomass-burning emissions. *Proc. Natl. Acad. Sci. U.S.A.* **2016**, *113*, 10013−10018.
(23) Kumar, N. K.; Corbin, J. C.; Bruns, E. A.; Massabó, D.; Slowik, J. G.; Drinovec, L.; Močnik, G.; Prati, P.; Vlachou, A.; Baltensperger, U.; Gysel, M.; El-Haddad, I.; Prévôt, A. S. H. Production of particulate brown carbon during atmospheric aging of residential wood-burning emissions. *Atmos. Chem. Phys.* **2018**, *18*, 17843.
(24) Laskin, A.; Laskin, J.; Nizkorodov, S. A. Chemistry of atmospheric brown carbon. *Chem. Rev.* **2015**, *115*, 4335−4382.
(25) He, Q.; Bluvshtein, N.; Segev, L.; Meidan, D.; Flores, J. M.; Brown, S. S.; Brune, W.; Rudich, Y. Evolution of the complex refractive index of secondary organic aerosols during atmospheric aging. *Environ. Sci. Technol.* **2018**, *52*, 3456−3465.
(26) Zhang, X.; Lin, Y. H.; Surratt, J. D.; Zotter, P.; Prévôt, A. S.; Weber, R. J. Light-absorbing soluble organic aerosol in Los Angeles and Atlanta: A contrast in secondary organic aerosol. *Geophys. Res. Lett.* **2011**, *38*, L21810.
(27) Yan, C.; Zheng, M.; Bosch, C.; Andersson, A.; Desyaterik, Y.; Sullivan, A. P.; Collett, J. L.; Zhao, B.; Wang, S.; He, K.; Gustafsson, Ö. Important fossil source contribution to brown carbon in Beijing during winter. *Sci. Rep.* **2017**, *7*, 43182.
(28) Huang, R.-J.; Yang, L.; Cao, J.; Chen, Y.; Chen, Q.; Li, Y.; Duan, J.; Zhu, C.; Dai, W.; Wang, K.; Lin, C.; Ni, H.; Corbin, J. C.; Wu, Y.; Zhang, R.; Tie, X.; Hoffmann, T.; O'Dowd, C.; Dusek, U. Brown carbon aerosol in urban Xi'an, northwest China: The composition and light absorption properties. *Environ. Sci. Technol.* **2018**, *52*, 6825−6833.
(29) Lin, P.; Fleming, L. T.; Nizkorodov, S. A.; Laskin, J.; Laskin, A. Comprehensive molecular characterization of atmospheric brown carbon by high resolution mass spectrometry with electrospray and atmospheric pressure photoionization. *Anal. Chem.* **2018**, *90*, 12493−12502.
(30) Saleh, R. From Measurements to Models: Toward Accurate Representation of Brown Carbon in Climate Calculations. *Curr. Pollut. Rep.* **2020**, *6*, 90−104.
(31) Wang, X.; Heald, C. L.; Ridley, D. A.; Schwarz, J. P.; Spackman, J. R.; Perring, A. E.; Coe, H.; Liu, D.; Clarke, A. D. Exploiting simultaneous observational constraints on mass and absorption to estimate the global direct radiative forcing of black carbon and brown carbon. *Atmos. Chem. Phys.* **2014**, *14*, 10989.
(32) Jo, D. S.; Park, R. J.; Lee, S.; Kim, S.-W.; Zhang, X. A global simulation of brown carbon: implications for photochemistry and direct radiative effect. *Atmos. Chem. Phys.* **2016**, *16*, 3413−3432.
(33) Pandey, A.; Hsu, A.; Tiwari, S.; Pervez, S.; Chakrabarty, R. K. Light absorption by organic aerosol emissions rivals that of black carbon from residential biomass fuels in South Asia. *Environ. Sci. Technol. Lett.* **2020**, *7*, 266−272.
(34) Yan, J.; Wang, X.; Gong, P.; Wang, C.; Cong, Z. Review of brown carbon aerosols: Recent progress and perspectives. *Sci. Total Environ.* **2018**, *634*, 1475−1485.
(35) Forrister, H.; Liu, J.; Scheuer, E.; Dibb, J.; Ziemba, L.; Thornhill, K. L.; Anderson, B.; Diskin, G.; Perring, A. E.; Schwarz, J. P.; Campuzano-Jost, P.; Day, D. A.; Palm, B. B.; Jimenez, J. L.; Nenes, A.; Weber, R. J. Evolution of brown carbon in wildfire plumes. *Geophys. Res. Lett.* **2015**, *42*, 4623−4630.
(36) Wang, X.; Heald, C. L.; Sedlacek, A. J.; de Sá, S. S.; Martin, S. T.; Alexander, M. L.; Watson, T. B.; Aiken, A. C.; Springston, S. R.; Artaxo, P. Deriving brown carbon from multiwavelength absorption measurements: method and application to AERONET and Aethalometer observations. *Atmos. Chem. Phys.* **2016**, *16*, 12733−12752.

https://doi.org/10.1021/acs.est.0c08706
Environ. Sci. Technol. XXXX, XXX, XXX−XXX

(37) Sumlin, B. J.; Pandey, A.; Walker, M. J.; Pattison, R. S.; Williams, B. J.; Chakrabarty, R. K. Atmospheric photooxidation diminishes light absorption by primary brown carbon aerosol from biomass burning. *Environ. Sci. Technol. Lett.* **2017**, *4*, 540−545.
(38) Solomon, P. A.; Crumpler, D.; Flanagan, J. B.; Jayanty, R. K. M.; Rickman, E. E.; McDade, C. E. US national $PM_{2.5}$ chemical speciation monitoring networks—CSN and IMPROVE: Description of networks. *J. Air Waste Manage. Assoc.* **2014**, *64*, 1410−1438.
(39) Tørseth, K.; Aas, W.; Breivik, K.; Fjæraa, A. M.; Fiebig, M.; Hjellbrekke, A. G.; Lund Myhre, C.; Solberg, S.; Yttri, K. E. Introduction to the European Monitoring and Evaluation Programme (EMEP) and observed atmospheric composition change during 1972−2009. *Atmos. Chem. Phys.* **2012**, *12*, 5447−5481.
(40) Xin, J.; Wang, Y.; Pan, Y.; Ji, D.; Liu, Z.; Wen, T.; Wang, Y.; Li, X.; Sun, Y.; Sun, J.; Wang, P.; Wang, G.; Wang, X.; Cong, Z.; Song, T.; Hu, B.; Wang, L.; Tang, G.; Gao, W.; Guo, Y.; Miao, H.; Tian, S.; Wang, L. The campaign on atmospheric aerosol research network of China: CARE-China. *Bull. Am. Meteorol. Soc.* **2015**, *96*, 1137−1155.
(41) Murphy, D. M.; Chow, J. C.; Leibensperger, E. M.; Malm, W. C.; Pitchford, M.; Schichtel, B. A.; Watson, J. G.; White, W. H. Decreases in elemental carbon and fine particle mass in the United States. *Atmos. Chem. Phys.* **2011**, *11*, 4679−4686.
(42) Chow, J. C.; Watson, J. G.; Doraiswamy, P.; Chen, L.-W. A.; Sodeman, D. A.; Lowenthal, D. H.; Park, K.; Arnott, W. P.; Motallebi, N. Aerosol light absorption, black carbon, and elemental carbon at the Fresno Supersite, California. *Atmos. Res.* **2009**, *93*, 874−887.
(43) Lack, D. A.; Moosmüller, H.; McMeeking, G. R.; Chakrabarty, R. K.; Baumgardner, D. Characterizing elemental, equivalent black, and refractory black carbon aerosol particles: a review of techniques, their limitations and uncertainties. *Anal. Bioanal. Chem.* **2014**, *406*, 99−122.
(44) Chow, J. C.; Watson, J. G.; Chen, L.-W. A.; Chang, M. C. O.; Robinson, N. F.; Trimble, D.; Kohl, S. The IMPROVE_A temperature protocol for thermal/optical carbon analysis: maintaining consistency with a long-term database. *J. Air Waste Manage. Assoc.* **2007**, *57*, 1014−1023.
(45) Chen, L.-W. A.; Chow, J. C.; Watson, J. G.; Schichtel, B. A. Consistency of long-term elemental carbon trends from thermal and optical measurements in the IMPROVE network. *Atmos. Meas. Tech.* **2012**, *5*, 2329.
(46) Chen, L.-W. A.; Chow, J. C.; Wang, X. L.; Robles, J. A.; Sumlin, B. J.; Lowenthal, D. H.; Zimmermann, R.; Watson, J. G. Multi-wavelength optical measurement to enhance thermal/optical analysis for carbonaceous aerosol. *Atmos. Meas. Tech.* **2015**, *8*, 451−461.
(47) Chow, J. C.; Wang, X.; Sumlin, B. J.; Gronstal, S. B.; Chen, L.-W. A.; Trimble, D. L.; Watson, J. G.; Kohl, S. D.; Mayorga, S. R.; Riggio, G.; Hurbain, P. R.; Johnson, M.; Zimmermann, R. Optical calibration and equivalence of a multiwavelength thermal/optical carbon analyzer. *Aerosol Air Qual. Res.* **2015**, *15*, 1145−1159.
(48) Chow, J. C.; Watson, J. G.; Green, M. C.; Wang, X.; Chen, L.-W. A.; Trimble, D. L.; Cropper, P. M.; Kohl, S. D.; Gronstal, S. B. Separation of brown carbon from black carbon for IMPROVE and Chemical Speciation Network $PM_{2.5}$ samples. *J. Air Waste Manage. Assoc.* **2018**, *68*, 494−510.
(49) Chow, J. C.; Watson, J. G.; Chen, L.-W. A.; Arnott, W. P.; Moosmüller, H.; Fung, K. Equivalence of elemental carbon by thermal/optical reflectance and transmittance with different temperature protocols. *Environ. Sci. Technol.* **2004**, *38*, 4414−4422.
(50) Cavalli, F.; Viana, M.; Yttri, K. E.; Genberg, J.; Putaud, J.-P. Toward a standardised thermal-optical protocol for measuring atmospheric organic and elemental carbon: the EUSAAR protocol. *Atmos. Meas. Tech.* **2010**, *3*, 79−89.
(51) Subramanian, R.; Khlystov, A. Y.; Robinson, A. L. Effect of peak inert-mode temperature on elemental carbon measured using thermal-optical analysis. *Aerosol Sci. Technol.* **2006**, *40*, 763−780.
(52) Cheng, Y.; Duan, F.-k.; He, K.-b.; Du, Z.-y.; Zheng, M.; Ma, Y.-l. Intercomparison of thermal-optical method with different temperature protocols: Implications from source samples and solvent extraction. *Atmos. Environ.* **2012**, *61*, 453−462.
(53) Malm, W. C.; Schichtel, B. A.; Hand, J. L.; Prenni, A. J. Implications of organic mass to carbon ratios increasing over time in the rural United States. *J. Geophys. Res.: Atmos.* **2020**, *125*, No. e2019JD031480.
(54) Chow, J. C.; Watson, J. G.; Robles, J.; Wang, X.; Chen, L.-W. A.; Trimble, D. L.; Kohl, S. D.; Tropp, R. J.; Fung, K. K. Quality assurance and quality control for thermal/optical analysis of aerosol samples for organic and elemental carbon. *Anal. Bioanal. Chem.* **2011**, *401*, 3141−3152.
(55) Chen, L.-W. A.; Chow, J. C.; Watson, J. G.; Moosmüller, H.; Arnott, W. P. Modeling reflectance and transmittance of quartz-fiber filter samples containing elemental carbon particles: Implications for thermal/optical analysis. *J. Aerosol Sci.* **2004**, *35*, 765−780.
(56) Chow, J. C.; Chen, L.-W. A.; Wang, X.; Green, M. C.; Watson, J. G. Improved estimation of $PM_{2.5}$ brown carbon contributions to filter light attenuation. *Particuology* **2021**, *56*, 1.
(57) Fujita, E. M.; Campbell, D. E.; Arnott, W. P.; Chow, J. C.; Zielinska, B. Evaluations of the chemical mass balance method for determining contributions of gasoline and diesel exhaust to ambient carbonaceous aerosols. *J. Air Waste Manage. Assoc.* **2007**, *57*, 721−740.
(58) Khan, B.; Hays, M. D.; Geron, C.; Jetter, J. Differences in the OC/EC ratios that characterize ambient and source aerosols due to thermal-optical analysis. *Aerosol Sci. Technol.* **2012**, *46*, 127−137.
(59) Watson, J. G.; Cooper, J. A.; Huntzicker, J. J. The effective variance weighting for least squares calculations applied to the mass balance receptor model. *Atmos. Environ.* **1984**, *18*, 1347−1355.
(60) Watson, J. G.; Chow, J. C.; Lowenthal, D. H.; Antony Chen, L.-W.; Shaw, S.; Edgerton, E. S.; Blanchard, C. L. $PM_{2.5}$ source apportionment with organic markers in the Southeastern Aerosol Research and Characterization (SEARCH) study. *J. Air Waste Manage. Assoc.* **2015**, *65*, 1104−1118.
(61) Watson, J. G.; Chow, J. C.; Chen, L.-W. A.; Engling, G.; Wang, X. L. Source Apportionment: Principles and Methods. *Airborne Particulate Matter: Sources, Atmospheric Processes and Health* **2016**, *42*, 72.
(62) Chen, L.-W. A.; Cao, J. $PM_{2.5}$ source apportionment using a hybrid environmental receptor model. *Environ. Sci. Technol.* **2018**, *52*, 6357−6369.
(63) Tian, J.; Wang, Q.; Han, Y.; Ye, J.; Wang, P.; Pongpiachan, S.; Ni, H.; Zhou, Y.; Wang, M.; Zhao, Y.; Cao, J. Contributions of aerosol composition and sources to particulate optical properties in a southern coastal city of China. *Atmos. Res.* **2020**, *235*, 104744.
(64) Saleh, R.; Cheng, Z.; Atwi, K. The brown−black continuum of light-absorbing combustion aerosols. *Environ. Sci. Technol. Lett.* **2018**, *5*, 508−513.
(65) Corbin, J. C.; Czech, H.; Massabò, D.; de Mongeot, F. B.; Jakobi, G.; Liu, F.; Lobo, P.; Mennucci, C.; Mensah, A. A.; Orasche, J.; Pieber, S. M. Infrared-absorbing carbonaceous tar can dominate light absorption by marine-engine exhaust. *npj Clim. Atmos. Sci.* **2019**, *2*, 12.
(66) Arnott, W. P.; Hamasha, K.; Moosmüller, H.; Sheridan, P. J.; Ogren, J. A. Towards aerosol light-absorption measurements with a 7-wavelength aethalometer: Evaluation with a photoacoustic instrument and 3-wavelength nephelometer. *Aerosol Sci. Technol.* **2005**, *39*, 17−29.
(67) Collaud Coen, M.; Weingartner, E.; Apituley, A.; Ceburnis, D.; Fierz-Schmidhauser, R.; Flentje, H.; Henzing, J. S.; Jennings, S. G.; Moerman, M.; Petzold, A.; Schmid, O.; Baltensperger, U. Minimizing light absorption measurement artifacts of the Aethalometer: evaluation of five correction algorithms. *Atmos. Meas. Tech.* **2010**, *3*, 457−474.
(68) Feng, Y.; Ramanathan, V.; Kotamarthi, V. R. Brown carbon: a significant atmospheric absorber of solar radiation? *Atmos. Chem. Phys.* **2013**, *13*, 8607−8621.
(69) Saleh, R.; Marks, M.; Heo, J.; Adams, P. J.; Donahue, N. M.; Robinson, A. L. Contribution of brown carbon and lensing to the direct radiative effect of carbonaceous aerosols from biomass and biofuel burning emissions. *J. Geophys. Res.: Atmos.* **2015**, *120*, 10285.

https://doi.org/10.1021/acs.est.0c08706
Environ. Sci. Technol. XXXX, XXX, XXX−XXX

(70) Watson, J. G.; Chen, L.-W. A.; Chow, J. C.; Doraiswamy, P.; Lowenthal, D. H. Source apportionment: findings from the US supersites program. *J. Air Waste Manage. Assoc.* **2008**, *58*, 265−288.
(71) Briggs, N. L.; Long, C. M. Critical review of black carbon and elemental carbon source apportionment in Europe and the United States. *Atmos. Environ.* **2016**, *144*, 409−427.
(72) Schichtel, B. A.; Hand, J. L.; Barna, M. G.; Gebhart, K. A.; Copeland, S.; Vimont, J.; Malm, W. C. Origin of fine particulate carbon in the rural United States. *Environ. Sci. Technol.* **2017**, *51*, 9846−9855.
(73) Chen, L.-W. A.; Watson, J. G.; Chow, J. C.; Magliano, K. L. Quantifying $PM_{2.5}$ source contributions for the San Joaquin Valley with multivariate receptor models. *Environ. Sci. Technol.* **2007**, *41*, 2818−2826.
(74) Lee, S.; Russell, A. G.; Baumann, K. Source apportionment of fine particulate matter in the southeastern United States. *J. Air Waste Manage. Assoc.* **2007**, *57*, 1123−1135.
(75) Hand, J. L.; Schichtel, B. A.; Pitchford, M.; Malm, W. C.; Frank, N. H. Seasonal composition of remote and urban fine particulate matter in the United States. *J. Geophys. Res.: Atmos.* **2012**, *117*, D05209.
(76) Park, R. J.; Jacob, D. J.; Logan, J. A. Fire and biofuel contributions to annual mean aerosol mass concentrations in the United States. *Atmos. Environ.* **2007**, *41*, 7389−7400.
(77) Lee, S.; Liu, W.; Wang, Y.; Russell, A. G.; Edgerton, E. S. Source apportionment of $PM_{2.5}$: Comparing PMF and CMB results for four ambient monitoring sites in the southeastern United States. *Atmos. Environ.* **2008**, *42*, 4126−4137.
(78) Washenfelder, R. A.; Attwood, A. R.; Brock, C. A.; Guo, H.; Xu, L.; Weber, R. J.; Ng, N. L.; Allen, H. M.; Ayres, B. R.; Baumann, K.; Cohen, R. C.; Draper, D. C.; Duffey, K. C.; Edgerton, E.; Fry, J. L.; Hu, W. W.; Jimenez, J. L.; Palm, B. B.; Romer, P.; Stone, E. A.; Wooldridge, P. J.; Brown, S. S. Biomass burning dominates brown carbon absorption in the rural southeastern United States. *Geophys. Res. Lett.* **2015**, *42*, 653−664.
(79) Xie, M.; Hays, M. D.; Holder, A. L. Light-absorbing organic carbon from prescribed and laboratory biomass burning and gasoline vehicle emissions. *Sci. Rep.* **2017**, *7*, 7318.
(80) Liao, H.; Henze, D. K.; Seinfeld, J. H.; Wu, S.; Mickley, L. J. Biogenic secondary organic aerosol over the United States: Comparison of climatological simulations with observations. *J. Geophys. Res.: Atmos.* **2007**, *112*, D06201.
(81) Sindelarova, K.; Granier, C.; Bouarar, I.; Guenther, A.; Tilmes, S.; Stavrakou, T.; Müller, J.-F.; Kuhn, U.; Stefani, P.; Knorr, W. Global data set of biogenic VOC emissions calculated by the MEGAN model over the last 30 years. *Atmos. Chem. Phys.* **2014**, *14*, 9317−9341.
(82) Fox, J. *Robust Regression. Appendix to an R and S-Plus Companion to Applied Regression*; SAGE Publications, Inc.: Thousand Oaks, California, 2002.
(83) California Smoke Information. Friday, August 19, 2016—Widespread Smoke, 2016. https://californiasmokeinfo.blogspot.com/2016/08/friday-august-19-2016-widespread-smoke.html (retrieved July 28, 2020).
(84) Pachon, J. E.; Weber, R. J.; Zhang, X.; Mulholland, J. A.; Russell, A. G. Revising the use of potassium (K) in the source apportionment of $PM_{2.5}$. *Atmos. Pollut. Res.* **2013**, *4*, 14−21.
(85) June, N. A.; Wang, X.; Chen, L. W. A.; Chow, J. C.; Watson, J. G.; Wang, X.; Henderson, B. H.; Zheng, Y.; Mao, J. Spatial and Temporal Variability of Brown Carbon in the United States: Implications for Direct Radiative Effects. *Geophys. Res. Lett.* **2020**, *47*, No. e2020GL090332.

https://doi.org/10.1021/acs.est.0c08706
Environ. Sci. Technol. XXXX, XXX, XXX−XXX